

Optimal control for hybrid magnetically suspended flywheel rotor based on state feedback exact linearization model

Science Progress

2020, Vol. 103(3) 1–23

© The Author(s) 2020

Article reuse guidelines:

sagepub.com/journals-permissions

DOI: 10.1177/0036850420951389

journals.sagepub.com/home/sci

Tong Wen^{1,2}, Biao Xiang³  and Shilei Zhang¹

¹Research Institute for Frontier Science, Beihang University, Beijing, China

²Ningbo Institute of Technology, Beihang University, Ningbo, Zhejiang province, China

³Department of Mechanical Engineering, Hong Kong Polytechnic University, Kowloon, Hong Kong SAR, China

Abstract

For a hybrid magnetically suspended flywheel (MSFW) rotor suspended by permanent magnet biased active magnetic bearing (AMB) and passive magnetic bearing (PMB), the dynamic functions are nonlinear and coupling among different degrees of freedom (DOFs). In this article, the nonlinear dynamic functions in two controllable DOFs of the hybrid MSFW rotor are developed based on the equivalent magnetic circuit, and then the nonlinear dynamic function is linearized by using the state feedback exact linearization (SFEL) in order to minimize the coupling in two controllable DOFs. Furthermore, an optimal control based on the SFEL model is designed to reduce displacement runout and coupling among two controllable DOFs of the hybrid MSFW rotor at the rated speed. Finally, the simulation and experimental results validate the effectiveness of the optimal control based on SFEL model, and the stability of the hybrid MSFW rotor with an impulse-type disturbance is improved.

Keywords

Hybrid magnetically suspended flywheel, active magnetic bearing, passive magnetic bearing, state feedback exact linearization, optimal control

Introduction

The magnetically suspended flywheel (MSFW) suspended by the magnetic bearings (MBs) is regarded as a promising actuator to realize the attitude control of the

Corresponding author:

Biao Xiang, CF306, Department of Mechanical Engineering, Hong Kong Polytechnic University, Kowloon, Hong Kong SAR, China.

Email: thomas.biao@gmail.com



Creative Commons Non Commercial CC BY-NC: This article is distributed under the terms of the Creative Commons Attribution-NonCommercial 4.0 License (<https://creativecommons.org/licenses/by-nc/4.0/>)

which permits non-commercial use, reproduction and distribution of the work without further permission provided the original work is attributed as specified on the SAGE and Open Access pages (<https://us.sagepub.com/en-us/nam/open-access-at-sage>).

high-precision spacecraft because of its advantages on the long-lifetime, the micro-vibration, the lubrication-free, and so on.¹⁻⁴ The rotor part of MSFW has five degrees of freedom (DOFs) controlled by the MBs except the axial rotation driven by the motor. On the one hand, for the whole active MSFW, the rotor part is controlled by the active magnetic bearings (AMBs) in five DOFs.⁵⁻⁷ On the other hand, for the passive-active hybrid MSFW, some DOFs of hybrid MSFW rotor are controlled by the AMBs, but other DOFs are suspended by the passive magnetic bearings (PMBs) without power supply.^{8, 9} Therefore, the energy consumption of the hybrid MSFW is reduced greatly because the hybrid MSFW rotor is suspended by the PMBs in some DOFs. Furthermore, in order to further save the energy consumption of the AMB, a novel structure of the permanent magnet biased AMB different from the pure AMB^{10,11} is designed in this article. The bias permanent magnet (PM) ring not only provides the bias magnetic flux for the AMB by replacing the bias current of the pure AMB, but also generates magnetic forces to realize the passive suspension of the MSFW rotor in some DOFs. However, although the energy consumption is reduced by adopting this novel permanent magnet biased AMB in the hybrid MSFW, the magnetic flux superposition and coupling of the bias PM rings lead to nonlinear dynamics of hybrid MSFW rotor,¹² so the displacement runout of hybrid MSFW rotor would be amplified. Moreover, the control precision on angular moment of the flywheel rotor is determined by its displacement runout in the attitude control of spacecraft,¹³ so the displacement runout of the MSFW rotor should be limited to improve the precision of the control torque. Therefore, the active control about nonlinear model of the hybrid MSFW rotor is critical to guarantee its stability, and then improve the control precision of angular moment applied to the spacecraft.

A series of control strategies had been applied to stabilize the MSFW rotor successfully. The sliding mode control (SMC)¹⁴ was used in the MSFW with a hybrid MB system, the maximum displacement deflection was restrained to 0.05 mm in radial direction, so the SMC model had good performance on suppressing the dynamic displacement of the MSFW rotor. The linear parameter-varying control was also used in the MSFW system to reduce the mean square error of rotor displacement at different rotational speeds.¹⁵ Moreover, the variable bias current control was proposed to save the energy consumption of the MSFW system.¹⁶ The linear quadratic gaussian optimal control was used in the MSFW system to suppress the gyroscopic coupling effect at high rotational speed.¹⁷ In addition, researchers also proposed other control methods to improve the control performance of the MSFW system such as the feedback linearization control,¹⁸⁻²¹ the inverse system method,^{22,23} the active vibration control^{24,25} and so on.

Those proposed control methods could obtain good control performance on the MSFW system with a pure AMB system. The bias magnetic flux and the control magnetic flux of the pure AMB are both provided by winding currents, and the coupling between the bias magnetic flux and the control magnetic flux is ignored by simplifying the bias magnetic flux into the equivalent bias current, so the decoupling model of the pure AMB is obtained. In addition, those proposed control

methods were designed based on the *Taylor linearization* (TL) model of the magnetic force, the nonlinear terms in dynamic function of the permanent magnet biased AMB were not analyzed and considered.

For the hybrid MSFW system, the magnetic forces generated by the permanent magnet biased AMB are coupling because the permanent magnet biased AMBs in different DOFs share a same PM ring. Thus, the translations of the MSFW rotor in two controllable DOFs are not only controlled by the permanent magnet biased AMBs, but also affected by the shared PM ring, so the dynamic model of the hybrid MSFW rotor is more complicated than whole active MSFW rotor.

In this article, an optimal control based on state feedback exact linearization (SFEL) model is designed to suppress the displacement runout of hybrid MSFW rotor. The SFEL model could realize the linearization of the magnetic force generated by the permanent magnet biased AMB in the hybrid MSFW rotor, and then the optimal control is applied to minimize the displacement runout of the hybrid MSFW rotor. So, the stability and the low consumption of the hybrid MSFW could be guaranteed. This paper is organized as follows. At first, the structure and prototype of the hybrid MSFW are introduced in section 2. The nonlinear coupling model of the hybrid MSFW rotor in two controllable DOFs is developed based on the equivalent magnetic circuit in section 3. In section 4, the nonlinear dynamic model is linearized exactly to a linear model based on SFEL model. The optimal control based on SFEL model is designed to realize the stable suspension of hybrid MSFW rotor in two controllable DOFs in section 5. Finally, the effectiveness of optimal control based on SFEL model of hybrid MSFW rotor is validated by simulations and experiments in section 6, the superior dynamic response and the better decoupling ability are obtained by decreasing displacement runout and control currents.

Structure of hybrid MSFW

As shown in Figure 1(a), the hybrid MSFW system consists of a rotor part, a stator part, a permanent magnet biased AMB, a PMB, a driving motor, a backup ball bearing, radial and axial displacement sensors, a seal cover and a basement. The whole hybrid MSFW rotor is sealed with an aluminum shell in order to increase the vacuum degree. The permanent magnet biased AMB and the PMB suspend the flywheel rotor at the equilibrium points in axial and radial directions. The permanent magnet synchronous motor (PMSM) is the driving motor to turn the hybrid MSFW rotor rotates around the axial principal axis. The backup ball bearing with 0.5 mm protective airgap is used to restrict the maximum displacement deflection of the hybrid MSFW rotor when the permanent magnet biased AMB is powered off. The displacement sensors mounted on stator part could measure dynamic displacements of the hybrid MSFW rotor in radial and axial directions.

The coordinate and motions with variable terms $[x \ y \ z \ \alpha \ \beta \ \Omega]$ on six DOFs of the hybrid MSFW rotor are shown in Figure 1(b). The rotational speed Ω around Z axis is controlled by the PMSM. The radial translations with displacement

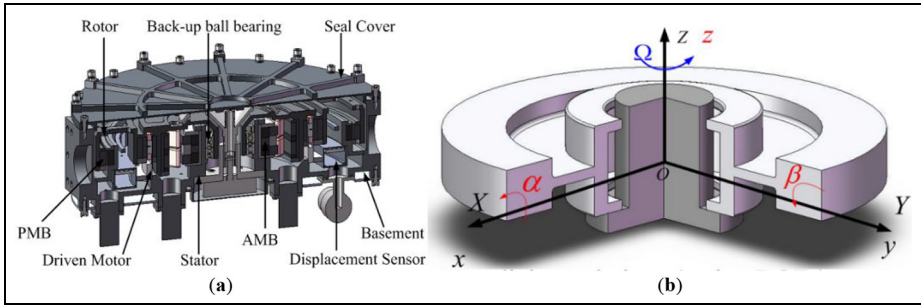


Figure 1. (a) The sketch of the hybrid MSFW system. (b) The rotor coordinate of the hybrid MSFW rotor.

variables x and y are controlled by the permanent magnet biased AMB and affected by the PMB. The radial rotations (rotational angle α around X axis and rotational angle β around Y axis) and the translation in Z axis (displacement term z) are passively controlled by the PMB when the hybrid MSFW rotor is suspended at the radial equilibrium position. Due to only two DOFs in radial translations are controlled by the permanent magnet biased AMB, the dynamic model and the control model in two controllable DOFs are developed, and the radial rotation of the hybrid MSFW rotor are analyzed according to the stiffness characteristics and magnetic torques of the PMB.

Model of hybrid MSFW

Magnetic force of permanent magnet biased AMB

Because the magnetic fluxes generated by the permanent magnet biased AMB and the PMB are not interlinked in the ferromagnetic steel embedded in the hybrid MSFW rotor, the magnetic forces generated by the permanent magnet biased AMB and the PMB could be calculated independently. For the permanent magnet biased AMB as shown in Figure 2(a), the magnetic forces acting on the hybrid MSFW rotor are generated by the magnetic fluxes of the bias PM ring and the coil currents in $X+$, $X-$, $Y+$, and $Y-$ directions. When the hybrid MSFW rotor suspends at the radial equilibrium position, the magnetic flux densities in four airgaps of the bias PM ring are identical, so the resultant magnetic forces of the bias PM ring acting on the hybrid MSFW rotor is zero. When the hybrid MSFW rotor deflects from the radial equilibrium position, the magnetic flux densities in four airgaps of the bias PM ring would be different, so the resultant magnetic forces of the bias PM ring acting on hybrid MSFW rotor is not zero. Therefore, the coil currents are tuned to balance magnetic flux densities in airgaps along four directions, and then magnetic forces make the hybrid MSFW rotor back to the equilibrium position.

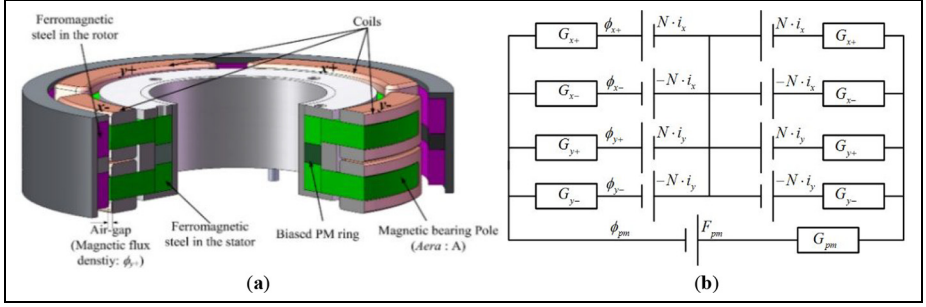


Figure 2. (a) The structure of permanent magnet biased AMB. (b) The equivalent magnetic circuit.

The equivalent magnetic circuit of the permanent magnet biased AMB is illustrated in Figure 2(b), the magnetic flux passes the ferromagnetic steel and airgap, finally returns to magnet pole. The coil currents in $X +$ and $X -$ directions are equal and opposite. According to the *Biot-Savart* law,²⁶ the magnetic forces f_{ex} and f_{ey} in X and Y axes are respectively expressed into

$$\begin{cases} f_{ex} = f_{ex+} - f_{ex-} = \frac{(\phi_{x+}^2 - \phi_{x-}^2)}{2\mu_0 A} \\ f_{ey} = f_{ey+} - f_{ey-} = \frac{(\phi_{y+}^2 - \phi_{y-}^2)}{2\mu_0 A} \end{cases} \quad (1)$$

where $f_{ex+}, f_{ex-}, f_{ey+}$ and f_{ey-} are magnetic forces generated by permanent magnet biased AMB. A is the cross-sectional area of single magnet pole. μ_0 is the vacuum permeability. $\phi_{x+}, \phi_{x-}, \phi_{y+}$ and ϕ_{y-} are magnetic flux densities along $X +, X -, Y +$ and $Y -$ directions, and

$$\begin{cases} \phi_{x-} = \frac{G_{x-} [2Ni_x (G_{x+} + G_{y+} + G_{y-} + G_{pm}) + 2Ni_x G_{x+} + 2Ni_y G_{y+} - 2Ni_y G_{y-} - F_{pm} G_{pm}]}{G} \\ \phi_{x+} = \frac{G_{x+} [2Ni_x (G_{x-} + G_{y+} + G_{y-} + G_{pm}) + 2Ni_x G_{x-} - 2Ni_y G_{y+} + 2Ni_y G_{y-} + F_{pm} G_{pm}]}{G} \\ \phi_{y-} = \frac{G_{y-} [2Ni_y (G_{y+} + G_{x+} + G_{x-} + G_{pm}) + 2Ni_y G_{y+} + 2Ni_x G_{x+} - 2Ni_x G_{x-} - F_{pm} G_{pm}]}{G} \\ \phi_{y+} = \frac{G_{y+} [2Ni_y (G_{y-} + G_{x+} + G_{x-} + G_{pm}) + 2Ni_y G_{y-} - 2Ni_x G_{x+} + 2Ni_x G_{x-} + F_{pm} G_{pm}]}{G} \\ \phi_{pm} = \frac{G_{pm} [(F_{pm} + 2Ni_x) G_{x+} + (F_{pm} - 2Ni_x) G_{x-} + (F_{pm} + 2Ni_y) G_{y+} + (F_{pm} - 2Ni_y) G_{y-}]}{G} \end{cases} \quad (2)$$

where G_{pm} is the magnetic conductance of the bias PM ring, F_{pm} is the magnetic potential of the bias PM ring, and they are

$$\begin{cases} G_{pm} = \frac{\mu_0 \mu_r A_{pm}}{h_{pm}} \\ F_{pm} = H_c h_{pm} \end{cases} \quad (3)$$

where H_c is the coercive force of the bias PM ring. A_{pm} is the cross-sectional area of the bias PM ring. h_{pm} is the length of the bias PM ring along the magnetization direction. μ_r is the relative vacuum permeability. i_x and i_y are control currents. N is the number of turns of single winding. g is the bias airgap of the bias PM ring. The length of the bias PM ring along the magnetization direction is 5 mm, and the maximum airgap of the bias PM ring is 0.3 mm, so there is

$$G_{pm} \ll G_{x+} + G_{x-} + G_{y+} + G_{y-} \quad (4)$$

And then

$$G = G_{x+} + G_{x-} + G_{y+} + G_{y-} + G_{pm} \approx G_{x+} + G_{x-} + G_{y+} + G_{y-} \quad (5)$$

The magnetic conductance in four airgaps are

$$\begin{cases} G_{x+} = \frac{\mu_0 A}{(g+x)}, G_{x-} = \frac{\mu_0 A}{(g-x)} \\ G_{y+} = \frac{\mu_0 A}{(g+y)}, G_{y-} = \frac{\mu_0 A}{(g-y)} \end{cases} \quad (6)$$

The magnetic forces could be expressed into

$$\begin{cases} f_{ex} = k_{11} \cdot i_x^2 + k_{12} \cdot i_x i_y + k_{13} \cdot i_y^2 + k_{14} \cdot i_x + k_{15} \cdot i_y + k_{16} \cdot x \\ f_{ey} = k_{21} \cdot i_x^2 + k_{22} \cdot i_x i_y + k_{23} \cdot i_y^2 + k_{24} \cdot i_x + k_{25} \cdot i_y + k_{26} \cdot y \end{cases} \quad (7)$$

where $k_{11} \sim k_{16}$ are coefficients of magnetic force f_{ex} , and $k_{21} \sim k_{26}$ are coefficients of magnetic force f_{ey} .

Those coefficients ($k_{11} \sim k_{16}$) of magnetic force are variable with radial displacements of the hybrid MSFW rotor. Considering the radial symmetry of the permanent magnet biased AMB, the coefficients of magnetic force f_{ex} are chosen as example, and relationships among coefficients $k_{11} \sim k_{16}$ and radial displacements are presented in Figure 3. The second-order coefficients (k_{11} , k_{12} , and k_{13}) are much less than the first-order coefficients (k_{14} , k_{15} , and k_{16}) with small control currents, so the second-order coefficients (k_{11} , k_{12} , and k_{13}) could be neglected in the dynamic model of the hybrid MSFW rotor. So, the magnetic forces f_{ex} and f_{ey} along X and Y axes are respectively expressed into

$$\begin{aligned} f_{ex} &= \frac{2NF_{pm}G_{pm}(g^2 - y^2)(2g^2 + x^2 - y^2)}{g(2g^2 - x^2 - y^2)^2} i_x - \frac{4NF_{pm}G_{pm}(g^2 - y^2)xy}{g(2g^2 - x^2 - y^2)^2} i_y \\ &\quad - \frac{(F_{pm}G_{pm})^2(g^2 - y^2)^2}{\mu_0 Ag(2g^2 - x^2 - y^2)^2} x \\ &= k_{14} \cdot i_x + k_{15} \cdot i_y + k_{16} \cdot x \end{aligned} \quad (8)$$

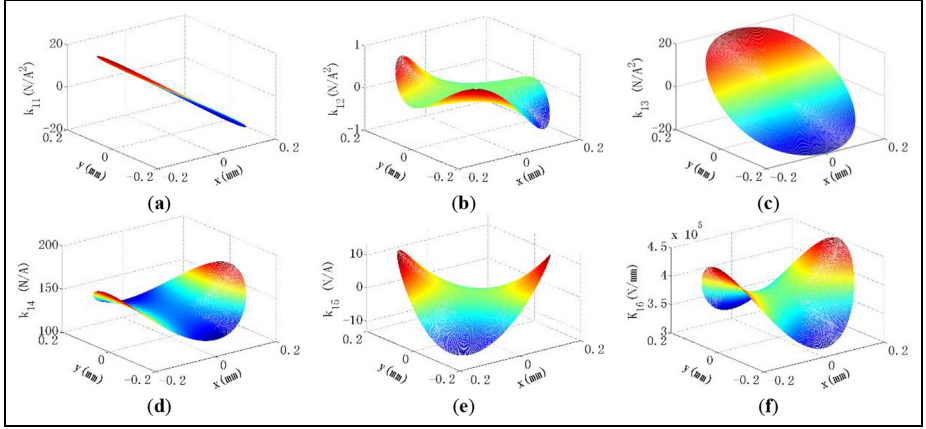


Figure 3. The relationships among coefficients $k_{11} \sim k_{16}$ of magnetic force f_{ex} , displacement deflection in X and Y axis. (a) Coefficient k_{11} . (b) Coefficient k_{12} . (c) Coefficient k_{13} . (d) Coefficient k_{14} . (e) Coefficient k_{15} . (f) Coefficient k_{16} .

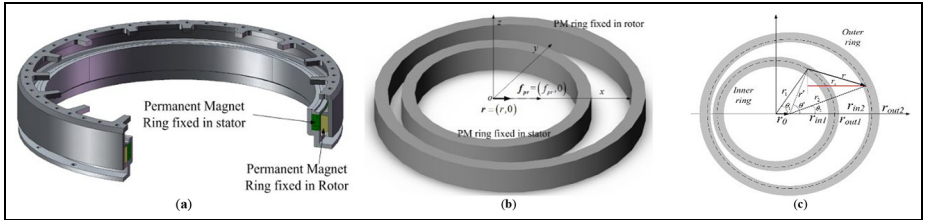


Figure 4. (a) The structure of the PMB. (b) The coordinate of the PMB. (c) The displacement variation of the PMB.

$$\begin{aligned}
 f_{ey} &= \frac{2NF_{pm}G_{pm}(g^2 - x^2)(2g^2 + y^2 - x^2)}{g(2g^2 - x^2 - y^2)^2}i_y - \frac{4NF_{pm}G_{pm}(g^2 - x^2)xy}{g(2g^2 - x^2 - y^2)^2}i_x \\
 &\quad - \frac{(F_{pm}G_{pm})^2(g^2 - x^2)^2}{\mu_0Ag(2g^2 - x^2 - y^2)^2}y \\
 &= k_{24} \cdot i_y + k_{25} \cdot i_x + k_{26} \cdot y
 \end{aligned} \tag{9}$$

Magnetic force of PMB

As shown in Figure 4(a), the PMB consists of one PM stator ring and one PM rotor ring with axial magnetization. Since that the angle range of radial rotation caused by the PMB is small, the coupling between radial translations and radial rotations could be neglected. The axial translation of the hybrid MSFW rotor is determined

by the component of gravity along Z axis, so the hybrid MSFW rotor would deflect from the axial equilibrium point when the component of gravity along Z axis is not zero, the magnetic force of the PMB could be further affected by axial displacement deflection. The magnetic force of the PMB²⁷ could be written into

$$\mathbf{F} = \frac{1}{4\pi\mu_0} \frac{Q_s Q_r}{r^3} \mathbf{r} \quad (10)$$

where Q_s and Q_r are magnetic charges of two PM rings, respectively, and \mathbf{r} is the eccentricity vector of two PM rings. The magnetic force f_{pr} of the PMB is determined by the eccentricity of two PM rings $\mathbf{r} = (r, \theta)$, and affected by the axial displacement deflection. As shown in Figure 4(b), the eccentricity of two PM rings in polar coordinate is expressed into

$$\begin{aligned} r &= \sqrt{x^2 + y^2} \\ \theta &= \arctan\left(\frac{y}{x}\right) \end{aligned} \quad (11)$$

The direction of magnetic force f_{pr} is consistent with the angle θ , and the amplitude of magnetic force f_{pr} is determined by the radius r and affected by the axial displacement deflection. The magnetic forces f_{px} and f_{py} in X and Y axes are respectively

$$\begin{cases} f_{px} = f_{pr} \cdot \cos \theta \\ f_{py} = f_{pr} \cdot \sin \theta \end{cases} \quad (12)$$

Since the PMB is symmetric about axial axis, the eccentricity of two PM rings is $\mathbf{r} = (r, 0)$ when only motion in Y axis happens, the magnetic force of the PMB could be expressed into

$$\begin{aligned} f_{pr} &= 2 \int_0^{2\pi} \int_0^{2\pi} \int_{r_{in1}}^{r_{out1}} \int_{r_{in2}}^{r_{out2}} r_x \frac{\sigma^* \sigma^*}{4\pi\mu_0} \frac{1}{r^3} r_1 r_2 dr_1 dr_2 d\theta_1 d\theta_2 \\ &\quad - 2 \int_0^{2\pi} \int_0^{2\pi} \int_{r_{in1}}^{r_{out1}} \int_{r_{in2}}^{r_{out2}} r_x \frac{\sigma^* \sigma^*}{4\pi\mu_0} \frac{1}{\tilde{r}^3} r_1 r_2 dr_1 dr_2 d\theta_1 d\theta_2 \end{aligned} \quad (13)$$

where σ^* is magnet pole surface density, r_{in1} is the inside radius of PM stator ring, r_{in2} is the inside radius of PM rotor ring, r_{out1} is the external radius of PM stator ring, r_{out2} is the external radius of PM rotor ring. The geometric relationship in Figure 4(c) is obtained as following

$$\begin{cases} r^2 = r_2^2 + r_1^2 + r_0^2 - 2r_0 r_1 \cos \theta_1 - 2r' r_2 \cos \theta' \\ \tilde{r}^2 = r_2^2 + r_1^2 + r_0^2 - 2r_0 r_1 \cos \theta_1 - 2r' r_2 \cos \theta' + h_{pmb}^2 \\ r_x = r_2 \cos \theta_2 - (r_1 \cos \theta_1 - r_0) \\ r' = \sqrt{r_1^2 + r_0^2 - 2r_0 r_1 \cos \theta_1} \end{cases} \quad (14)$$

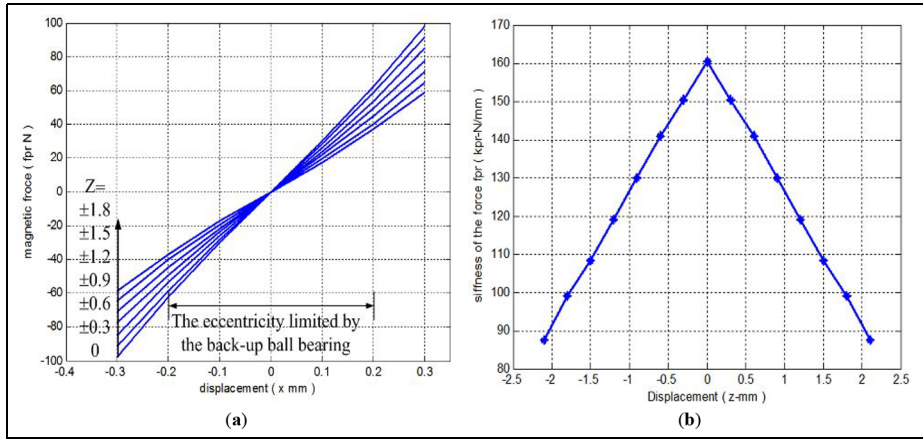


Figure 5. (a) Magnetic force of the PMB versus radial displacement. (b) Stiffness of the PMB versus radial displacement.

The curve of the magnetic force f_{pr} versus the radial displacement r is plotted in Figure 5(a) when the axial displacement varies from -1.8 mm to 1.8 mm. The eccentricity of two PM rings is less than 0.2 mm because of restriction of auxiliary backup ball bearing, so the magnetic force of the PMB could be expressed into a linear function with the displacement stiffness k_{pr} and the axial displacement z as following

$$k_{pr} = k_{pr0} - k_z \cdot |z| \quad (15)$$

where k_{pr0} is the radial stiffness of the PMB when the axial displacement z is zero.

As shown in Figure 5(b), the linearized magnetic forces of the PMB in radial directions are

$$\begin{cases} f_{pr} = (k_{pr0} - k_z \cdot |z|) \cdot r_0 = k_{pr} \cdot r_0 \\ f_{px} = f_{pr} \cos \theta = k_{pr} x \\ f_{py} = f_{pr} \sin \theta = k_{pr} y \end{cases} \quad (16)$$

When the hybrid MSFW system works in space, the micro-gravity environment ensures the MSFW rotor suspends at the axial equilibrium position without axial displacement deflection, the displacement stiffness of the PMB k_{pr} could be kept at a constant. For the experiment on the ground, the axial displacement is steady because of the fixed direction of the hybrid MSFW, so k_{pr} could be regarded as a constant referring to (15).

Dynamic model of hybrid MSFW rotor in two active DOFs

In Figure 1(b), dynamic equations of the hybrid MSFW rotor in two controllable DOFs are

$$\begin{cases} m\ddot{x} = f_{ex} + f_{px} + \Delta f_x \\ m\ddot{y} = f_{ey} + f_{py} + \Delta f_y \end{cases} \quad (17)$$

where Δf_x and Δf_y are disturbance forces, and m is the mass of the hybrid MSFW rotor.

The state variables are chosen as $\mathbf{X} = [x_1 x_2 x_3 x_4]^T = [x \ x' \ y \ y']^T$. The system inputs are control currents $\mathbf{u} = [u_1 \ u_2]^T = [i_x \ i_y]^T$. The system output are $\mathbf{Y} = [y_1 \ y_2]^T = [x \ y]^T$. Substituting (8), (9), and (16) into (17), the state space function is written into

$$\begin{cases} \dot{\mathbf{X}} = \mathbf{f}(\mathbf{X}) + \sum_{i=1}^2 \mathbf{g}_i(\mathbf{X})u_i + \Delta \\ \mathbf{Y} = \mathbf{h}(\mathbf{X}) \end{cases} \quad (18)$$

where $\mathbf{f}(\mathbf{X})$ is the state function, $\mathbf{g}_i(\mathbf{X})$ is the input function, and $\mathbf{h}(\mathbf{X})$ is the output function.

$$\begin{cases} f_1(\mathbf{X}) = x_2 \\ f_2(\mathbf{X}) = \frac{(k_{16}x_1 + k_{pr}x_1)}{m} \\ f_3(\mathbf{X}) = x_4 \\ f_4(\mathbf{X}) = \frac{(k_{26}x_3 + k_{pr}x_3)}{m} \end{cases} \quad (19)$$

$$\begin{cases} g_1(\mathbf{X}) = \frac{1}{m} [0 \ k_{14} \ 0 \ k_{15}]^T \\ g_2(\mathbf{X}) = \frac{1}{m} [0 \ k_{25} \ 0 \ k_{24}]^T \end{cases} \quad (20)$$

$$\begin{cases} y_1 = h_1(\mathbf{X}) = x_1 \\ y_2 = h_2(\mathbf{X}) = x_3 \end{cases} \quad (21)$$

Dynamic model of hybrid MSFW rotor in two passive DOFs

The rotational angles $[\alpha \ \beta]$ around radial axes of the hybrid MSFW rotor are dominated by the PMB only, so the rotational stability around radial axes is determined by the torque stiffness of the PMB, the range of rotational angle α is $[-1.2^\circ, 1.2^\circ]$ because of the limitation of backup ball bearing. Taking the rotation around X axis in Figure 6 for example. The PMB generates magnetic torque p_x when the hybrid MSFW rotor tilts an angle α around the equilibrium position. The calculation results of the magnetic torque p_x and the torque stiffness k_{px} are plotted in Figure 7, and the magnetic torque of the PMB has the restoring ability. When the hybrid MSFW rotor deflects from the radial equilibrium position, it could be pulled back to the equilibrium position by the magnetic torque with a negative

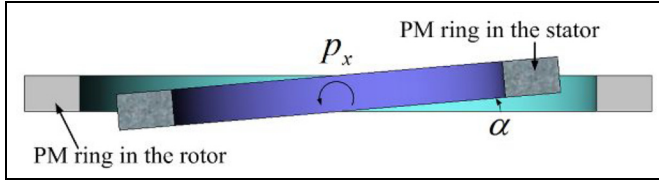


Figure 6. Radial rotation of the PMB around x axis.

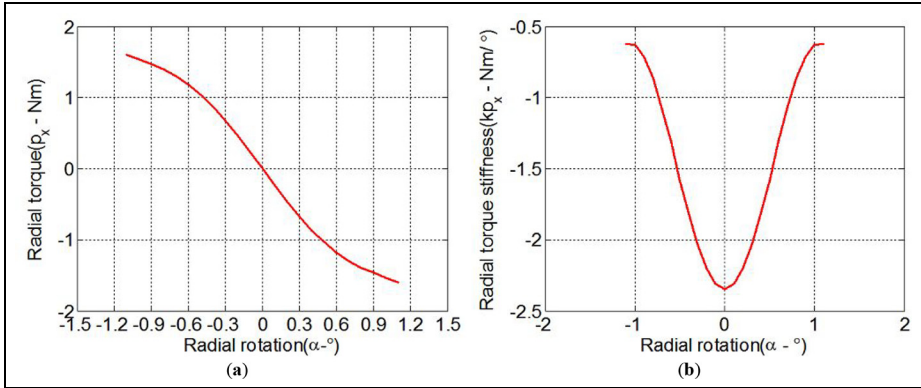


Figure 7. (a) The magnetic force of the PMB versus the radial displacement. (b) The torque stiffness of the PMB versus the radial displacement.

stiffness. Therefore, the radial rotations of hybrid MSFW rotor are naturally stable.

In the meanwhile, the radial rotations of hybrid MSFW rotor are affected by disturbance torques, and the primary disturbance in radial rotation is the residual couple unbalance. Due to the great torque stiffness of the PMB, the radial rotational angles of hybrid MSFW rotor are small at high rotational speed. As shown in Figure 8, the measured result of radial rotational angle is smaller than 0.02° when rotational speed is 5000 rpm. Therefore, the dynamic equations of radial translations could be decoupled from radial rotations, and influences acting on radial translation could be neglected.

State feedback exact linearization of hybrid MSFW rotor

The nonlinear model of the hybrid MSFW rotor in (18) is the conical form, so it could be linearized exactly to a linear model through the state feedback.^{28,29} The dynamic function of the hybrid MSFW rotor in (18) is a four-order affine nonlinear system with two inputs and two outputs, so its relative degree defined by the *Lie*-

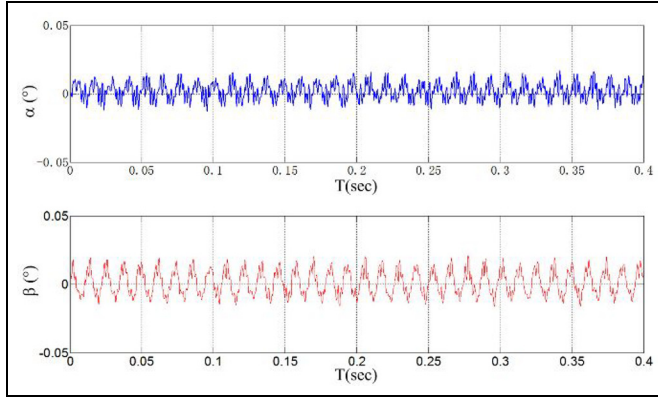


Figure 8. The radial rotational angles of the hybrid MSFW rotor at the rated speed 5000 rpm.

derivative is four within the vicinity of $X_0 = 0$. Therefore, the space state equation in (18) could be exactly linearized within the vicinity of $X_0 = 0$ through the state feedback.

Since the relative degree of nonlinear model is four, the matrix $A(X)$ in (22) is nonsingular within the vicinity of $X_0 = 0$.

$$A(X) = \begin{bmatrix} L_{g_1} L_f h_1(X) & L_{g_2} L_f h_1(X) \\ L_{g_1} L_f h_2(X) & L_{g_2} L_f h_2(X) \end{bmatrix} = \frac{1}{m} \begin{bmatrix} k_{14} & k_{25} \\ k_{15} & k_{24} \end{bmatrix} \quad (22)$$

Defining the matrix as

$$b(X) = \begin{bmatrix} L_f^2 h_1(X) \\ L_f^2 h_1(X) \end{bmatrix} = \frac{1}{m} \begin{bmatrix} (k_{16} + k_{pr})x_1 \\ (k_{26} + k_{pr})x_3 \end{bmatrix} \quad (23)$$

And following inputs are introduced into the nonlinear model

$$v = \begin{bmatrix} v_1 \\ v_2 \end{bmatrix} = b(X) + A(X)u \quad (24)$$

The nonlinear model could be transformed into a linear model with a standard *Brunovsky* form

$$\dot{X} = \bar{A}X + \bar{B}v \quad (25)$$

with state variables

$$\begin{aligned} \begin{bmatrix} \dot{x}_1 \\ \dot{x}_2 \end{bmatrix} &= \begin{bmatrix} 0 & 1 \\ 0 & 0 \end{bmatrix} \begin{bmatrix} x_1 \\ x_2 \end{bmatrix} + \begin{bmatrix} 0 \\ 1 \end{bmatrix} v_1 \\ \begin{bmatrix} \dot{x}_3 \\ \dot{x}_4 \end{bmatrix} &= \begin{bmatrix} 0 & 1 \\ 0 & 0 \end{bmatrix} \begin{bmatrix} x_3 \\ x_4 \end{bmatrix} + \begin{bmatrix} 0 \\ 1 \end{bmatrix} v_2 \end{aligned} \quad (26)$$

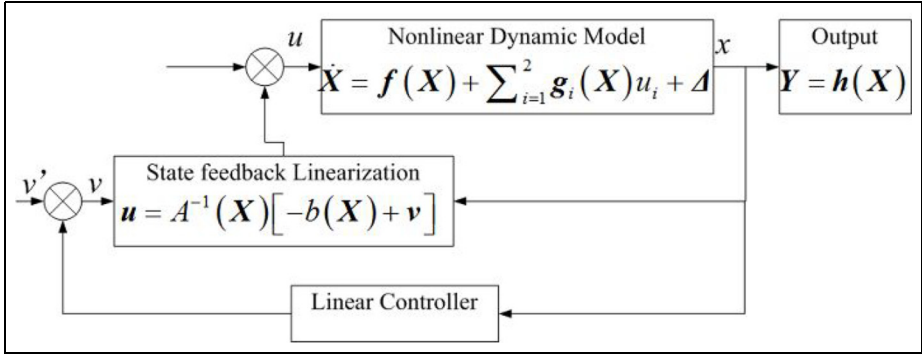


Figure 9. Control diagram of nonlinear hybrid MSFW rotor.

So real inputs applied to the original nonlinear model are

$$u = A^{-1}(X)[-b(X) + v] \quad (27)$$

Therefore, the SEFL model of the hybrid MSFW rotor has two signal input signal output (SISO) linear sub-systems.

Optimal control based on SFEL model of hybrid MSFW rotor

The control system designed for the hybrid MSFW rotor is illustrated in Figure 9. The optimal linear quadratic control is used to decouple the nonlinear model of the hybrid MSFW rotor. The measured displacements x and y are used as state variables. The cost function in (28) is chosen to evaluate the dynamic performance of the hybrid MSFW rotor.

$$J = \frac{1}{2} \int_0^{\infty} [X^T X + u^T u] dt \quad (28)$$

where $X^T X$ represents the state error, and $u^T u$ represents the power consumption.

Substituting (27) into $u^T u$ and neglecting $v^T A^{-T}(X)A^{-1}(X)b(X)$ and $b^T(X)A^{-T}(X)A^{-1}(X)v$, a standard cost function for the optimal control is obtained as following

$$\begin{aligned} u^T u &= [v - b(X)]^T A^{-T}(X)A^{-1}(X)[v - b(X)] \\ &\approx v^T [A(X)A^T(X)]^{-1} v + b(X)^T [A(X)A^T(X)]^{-1} b(X)^T \end{aligned} \quad (29)$$

It is obvious that (29) is nonlinear about the displacement of hybrid MSFW rotor, so the linear matrix of the cost function through *Taylor series* is achieved as following

$$\begin{aligned}
u^T u &\approx u^T u|_{X=0} + X^T \left[\frac{\partial}{\partial X} u^T u|_{X=0} \right] X \\
&= X^T \cdot \frac{\partial}{\partial X} \left\{ \begin{array}{l} v^T [A(X)A^T(X)]^{-1} v + \dots \\ b(X)^T [A(X)A^T(X)]^{-1} b(X) \end{array} \right\} \bigg|_{X=0} \cdot X = X^T [B_1 + B_2] X + v^T R v
\end{aligned} \tag{30}$$

where

$$R = \left(\frac{gm}{2NF_{pm}G_{pm}} \right)^2 \cdot I \tag{31}$$

$$B_1 = \left(\frac{gm}{NF_{pm}G_{pm}} \right)^2 \cdot \text{diag} \left[\left(\frac{-(F_{pm}G_{pm})^2}{4\mu_0 Agm} + \frac{k_{pr}}{m} \right)^2 \quad 0 \quad 0 \quad 0 \right] \tag{32}$$

$$B_2 = \left(\frac{gm}{NF_{pm}G_{pm}} \right)^2 \cdot \text{diag} \left[0 \quad 0 \quad \left(\frac{-(F_{pm}G_{pm})^2}{4\mu_0 Agm} + \frac{k_{pr}}{m} \right)^2 \quad 0 \right] \tag{33}$$

Substituting (30) into (28), the constant cost function for optimal control of linear model is

$$J = \frac{1}{2} \int_0^{\infty} [X^T (B_1 + B_2 + I) X + v^T R v] dt = \frac{1}{2} \int_0^{\infty} [X^T Q X + v^T R v] dt \tag{34}$$

where $Q = B_1 + B_2 + I$. The feedback law applied to the SFEL model is

$$v = -R^{-1} \bar{B}^T P X = F X \tag{35}$$

The matrix P is the solution of *Riccati* equation as following

$$P \bar{A} + \bar{A}^T P - P \bar{B} R^{-1} \bar{B}^T P + Q = 0 \tag{36}$$

Substituting (35) into (27), the feedback law for nonlinear model of the hybrid MSFW rotor is

$$u = A^{-1}(X) \left[-b(X) - R^{-1} \bar{B}^T P X \right] \tag{37}$$

Numerical simulation and experiment

Magnetic force of permanent magnet biased AMB

The hybrid MSFW rotor is not perfectly symmetric about mass distribution and geometry, so the unbalance term is not eliminated. When the hybrid MSFW rotor works at a high rotational speed, the periodical disturbance induced by the residual

Table 1. Parameters of hybrid MSFW rotor.

Symbol	Value	Symbol	Value	Symbol	Value	Symbol	Value
μ_r	1.05	r_{in1}	87.5 cm	h_{pm}	5 mm	A	259.8 mm ²
μ_0	$4\pi 10^{-7}$	r_{in2}	92.5 cm	A_{pm}	999 mm ²	H_c	4.810 ⁶ A/m
m	4.5 kg	r_{out1}	93.5 cm	g	0.6 mm	h_{pm}	10 mm
N	150	r_{out2}	98.5 cm	m_s	50 mg	ω	5000 rpm

imbalance could affect the stability of the hybrid MSFW rotor. The disturbance forces caused by the static imbalance mass are

$$\begin{cases} \Delta f_x = m_s R \omega^2 \cos(\omega t + \alpha_s) \\ \Delta f_y = m_s R \omega^2 \sin(\omega t + \alpha_s) \end{cases} \quad (38)$$

where R is the radius of the hybrid MSFW rotor, m_s is the static imbalance mass of the hybrid MSFW rotor, α_s is the location of imbalance mass, and ω is the rotational speed. The hybrid MSFW in the simulation and experiment is a prototype used in the attitude control of a middle-size satellite, and parameters are listed in Table 1. The angular moment of the hybrid MSFW is 25 Nm at 5000 rpm. The matrix \mathbf{P} in (36) is

$$\mathbf{P} = \begin{bmatrix} 1109.5 & 4.023 & 0 & 0 \\ 4.027 & 0.0329 & 0 & 0 \\ 0 & 0 & 1109.5 & 4.023 \\ 0 & 0 & 4.027 & 0.0329 \end{bmatrix} \quad (39)$$

And the closed-loop poles are $\lambda_{1,2} = -137.8 \pm 121.6i$, $\lambda_{3,4} = -137.8 \pm 121.6i$, so the control system of the hybrid MSFW rotor with the optimal control based on the SEFL model is stable.

The feedback law applied to the SFEL model calculated from (35) is

$$\mathbf{v} = -\mathbf{R}^{-1} \mathbf{B}^T \mathbf{P} \mathbf{X} = \begin{bmatrix} 3376.6 & 275.5 & 0 & 0 \\ 0 & 0 & 3376.6 & 275.5 \end{bmatrix} \mathbf{X} \quad (40)$$

Substituting the feedback law into (27), the actual inputs applied to the hybrid MSFW rotor are updated according to the system states.

In the simulation and experiment, the control performances of the PID control based on TL model and the optimal control based on SFEL model are compared. The initial states are $\mathbf{X} = [-1.5 \mu\text{m} \ 0 \ 1.2 \mu\text{m} \ 0]^T$, and the axial displacement of the hybrid MSFW rotor is 1.2 mm caused by the axial component of gravity. The magnetic forces of the permanent magnet biased AMB would make the hybrid MSFW rotor suspends at the equilibrium position. The suspension traces of the hybrid MSFW rotor are plotted in Figure 10(a), the hybrid MSFW rotor is stably suspended at radial equilibrium position when the dynamic displacements equal to

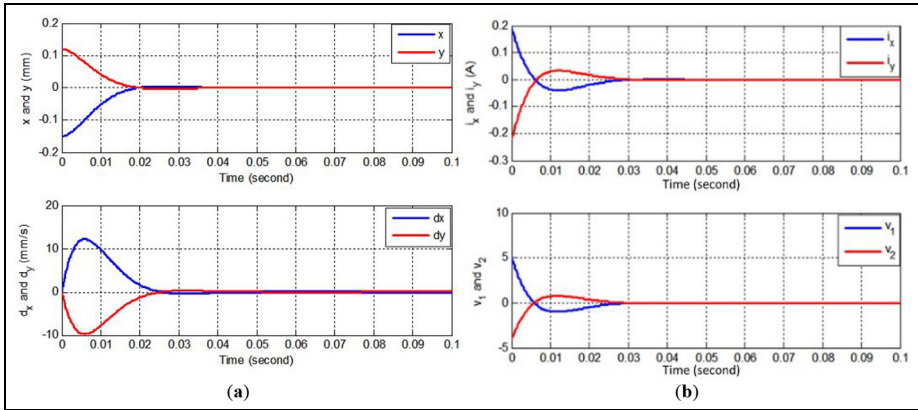


Figure 10. (a) The suspension traces of hybrid MSFW rotor. (b) The control currents of nonlinear and linearized model.

zero, and the settling time is 30 ms. Moreover, the control inputs i_x and i_y of the nonlinear model and the equivalent inputs v_1 and v_2 of the linearized model are depicted in Figure 10(b), there is no obvious difference between the nonlinear model and the linearized model, the comparison between control inputs of nonlinear model and equivalent inputs of linearized model indicates that the reference input could be accurately tracked by the linearized model.

The suspension traces of the hybrid MSFW rotor with a periodic disturbance and an impulse disturbance are plotted in Figure 11. For the suspension traces of PID control based on TL model as shown in Figure 11(a), the settling time for the periodic disturbance is 150 ms, and the settling time for the impulse disturbance is 15 ms with 50 μm amplitude. As illustrated in Figure 11(b), for the optimal control based on SFEL model, the settling time for the periodic disturbance is reduced to 30 ms, and the settling time for the impulse disturbance is 5 ms with 45 μm amplitude. Therefore, the simulation results show that the optimal control based on SFEL model has better anti-disturbance performance than the PID control based on TL model.

Experiment

The prototype of the hybrid MSFW with the permanent magnet biased AMB and the PMB is shown in Figure 12. The displacement sensors, winding of the permanent magnet biased AMB, PM stator ring of the PMB and windings of PMSM are mounted on the stator part of hybrid MSFW in Figure 12(b). The rotor part including the PM rotor ring and the hybrid MSFW rotor is shown in Figure 12(c). The whole experimental setup is displayed in Figure 13, the hybrid MSFW is sealed in a vacuum tank (pressure $< 5 \text{ Pa}$) to eliminate the influence caused by the wind drag at a high rotational speed. The main control unit (MCU) based on a

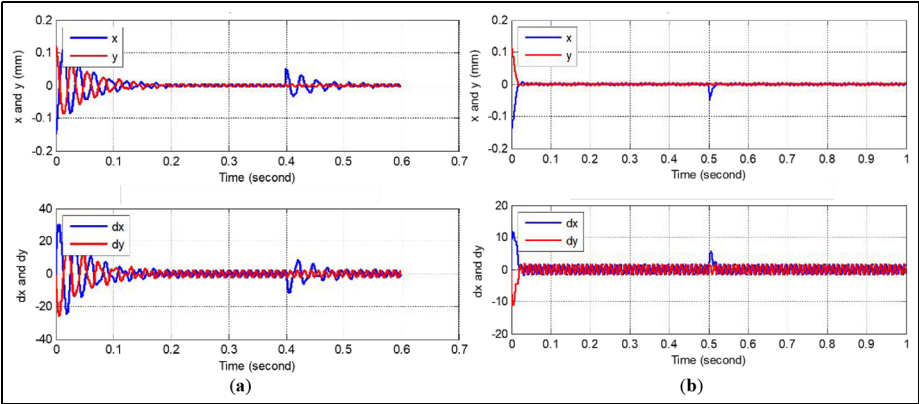


Figure 11. The suspension traces of hybrid MSFW rotor with periodic disturbance and impulse disturbances. (a) PID control based on TL model. (b) Optimal control based on SFEL model.

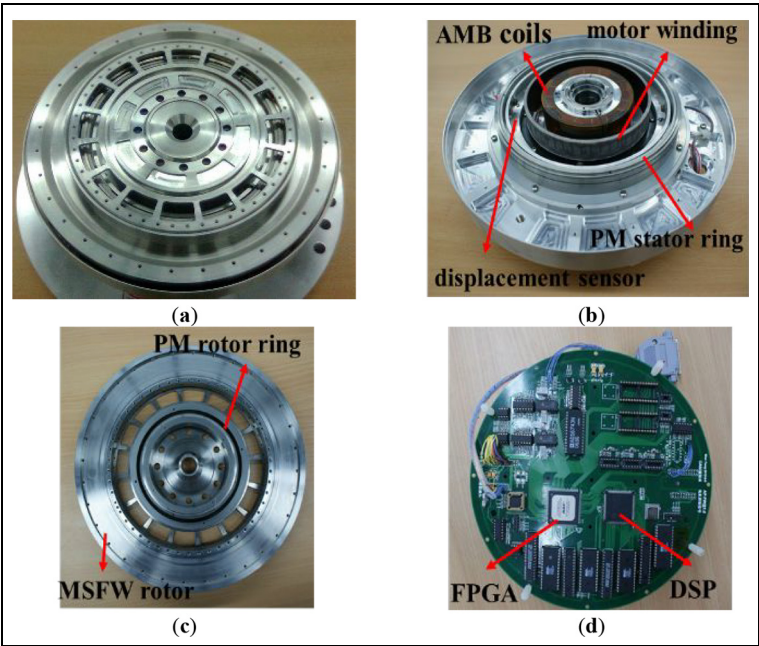


Figure 12. The prototype of hybrid MSFW. (a) Full view. (b) Stator part. (c) Rotor part. (d) MCU.

DSP chip and a FPGA chip could realize the control method programming and collect system signals such as dynamic displacements, control currents and rotational speed. The oscilloscope timely records and displays the dynamic displacements of the hybrid MSFW rotor.

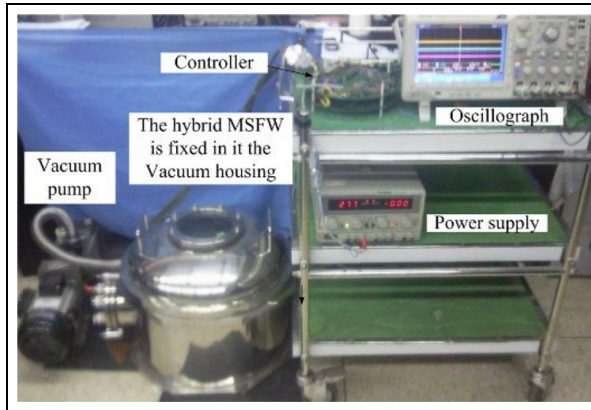


Figure 13. Control diagram of the hybrid MSFW rotor.

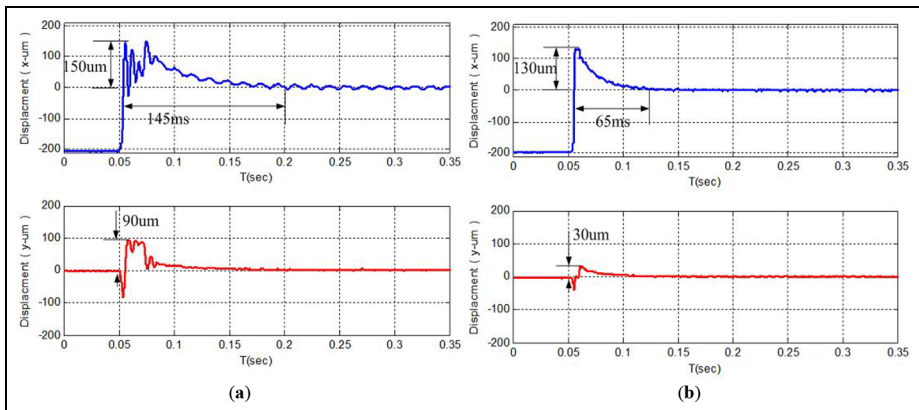


Figure 14. Suspension traces of the hybrid MSFW rotor. (a) With PID control based on TL model. (b) With optimal control based on SFEL model.

The initial displacement of the hybrid MSFW rotor sets at $X = [-200\mu\text{m } 0 \ 0]$, the suspension trace of the hybrid MSFW rotor with PID control based on TL model is plotted in Figure 14(a), and the suspension trace of the hybrid MSFW rotor with optimal control based on SFEL model is illustrated in Figure 14(b). The overshoot of suspension trace is reduced from $150\mu\text{m}$ to $130\mu\text{m}$, and the settling time is declined from 145ms to 65ms by using the optimal control based on SFEL model. In the meanwhile, the suspension trace of the hybrid MSFW rotor along Y axis is affected by the suspension process along X axis, and the oscillation peak is reduced from $90\mu\text{m}$ of PID control based on TL model to $30\mu\text{m}$ of the optimal control based on SFEL model. Therefore, the optimal control based on SFEL

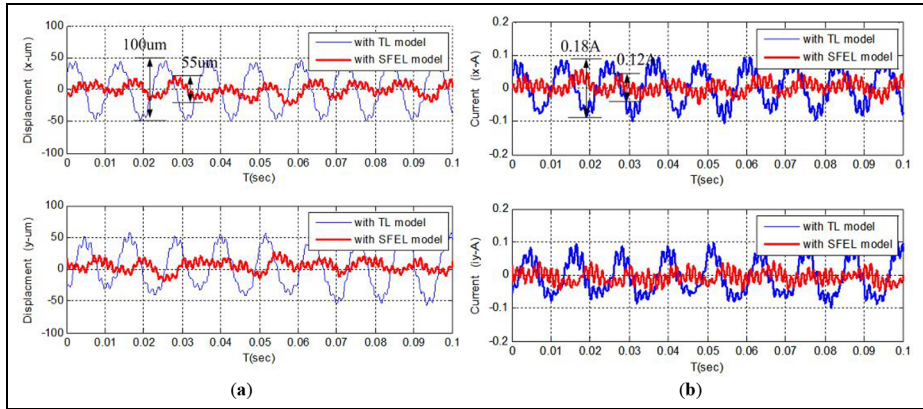


Figure 15. (a) Dynamic displacements of the hybrid MSFW rotor in X and Y axes at 5000 rpm. (b) Control currents i_x and i_y at 5000 rpm.

model not only has better dynamic performance, but also minimize the coupling between suspension traces along X and Y axes.

Moreover, the dynamic displacements of the hybrid MSFW rotor at 5000 rpm are plotted in Figure 15(a), the dynamic displacement of the hybrid MSFW rotor with PID control based on TL model is shown by the blue line, and dynamic displacement with optimal control based on SFEL model is marked by red line. The displacement runout (peak to peak value) of the hybrid MSFW rotor is used to evaluate the control performance, the smaller displacement runout, the better control performance. The displacement runout of the hybrid MSFW rotor is $55\text{ }\mu\text{m}$ with the optimal control based on SFEL model, but that of PID control based on TL model is $100\text{ }\mu\text{m}$. Figure 15(b) shows control currents i_x and i_y in control channels of X and Y axes when the hybrid MSFW rotor works at 5000 rpm. By applying the optimal control based on SFEL model, the control current (peak to peak value) is reduced from 0.18 A to 0.12 A . Therefore, the optimal control based on SFEL model has better performance on suppressing the displacement runout of the hybrid MSFW rotor at rated speed.

Referring to (7), there are coupling terms among dynamic equations of the hybrid MSFW rotor in different DOFs, so the disturbance acting on the suspension trace in Y axis also affects the dynamic displacements in X axis. The optimal control based on SFEL model is designed to minimize the coupling among two controllable DOFs of the hybrid MSFW rotor. The decoupling ability of the optimal control based on SFEL model and PID control based on TL model are compared when an impulse-type disturbance is imposed on suspension trace in X axis of the hybrid MSFW rotor at 5000 rpm. As illustrated in Figure 16, the dynamic displacement in X axis is obviously affected by the disturbance in Y axis, and both

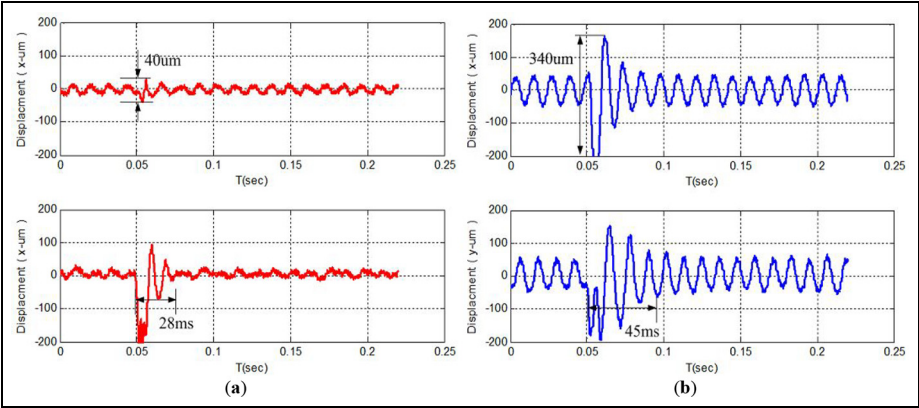


Figure 16. (a) Decoupling ability of optimal control based on SFEL model. (b) Decoupling ability of PID control based on TL model.

Table 2. Comparison between SFEL model and TL model.

	Suspension trace		Speed = 5000 rmp		Decoupling ability	
	TL model	SEFL model	TL model	SEFL model	TL model	SEFL model
Runout in X axis	150 μm	130 μm	100 μm	55 μm	340 μm	40 μm
Runout in Y axis	90 μm	30 μm				
Settling time	145 ms	65 ms			45 ms	28 ms
Control current			0.18 A	0.12 A		

of two control models could stabilize dynamic displacements of the hybrid MSFW rotor. For the PID control based on TL model, the displacement runout along X axis is 340 μm, the settling time back to the equilibrium position is 45 ms. The displacement runout along X axis is declined to 40 μm and the settling time is shortened to 28 ms by applying the optimal control based on SFEL model. Therefore, this result is consistent with simulation result that the optimal control based on SFEL model has better decoupling ability and anti-disturbance ability than the PID control based on TL model.

Conclusion

In this article, the nonlinear dynamic model of the hybrid MSFW rotor with the permanent magnet biased AMB and the PMB is developed, and then there are coupling terms in two controllable DOFs. Furthermore, an optimal control strategy based on SFEL model is designed to improve the decoupling ability in two

controllable DOFs and enhance the anti-disturbance ability of the hybrid MSFW rotor. As listed in Table 2, the simulation and experimental results prove that the optimal control based on SEFL model has better performance on decoupling and anti-disturbance when an impulse-style disturbance is imposed on the hybrid MSFW rotor at rated speed. Therefore, this control method is potential to be applied in control engineering of the hybrid MSFW used in attitude control of a middle-sized satellite.


Declaration of conflicting interests

The author(s) declared no potential conflicts of interest with respect to the research, authorship, and/or publication of this article.

Funding

The author(s) received no financial support for the research, authorship, and/or publication of this article.

ORCID iD

Biao Xiang  <https://orcid.org/0000-0002-0405-2030>

References

1. Rajagopal K and Sivadasan K. Low-stiction magnetic bearing for satellite application. *J Appl Phys* 2002; 91: 6994–6996.
2. Studer P. Magnetic bearings for spacecraft. *IEEE Trans Magn* 1971; 7: 520–520.
3. Morales W, Fusaro R and Kascak A. Permanent magnetic bearing for spacecraft applications. *Tribol Trans* 2003; 46: 460–464.
4. McLallin K, Jansen R, Fausz J, et al. Aerospace Flywheel Technology Development for IPACS Applications. 2001. DOI: 10.1115/IECEC2001-AT-82.
5. Xiang B and Tang J. Suspension and titling of vernier-gimballing magnetically suspended flywheel with conical magnetic bearing and Lorentz magnetic bearing. *Mechatronics* 2015; 28: 46–54.
6. Tezuka T, Kurita N and Ishikawa T. Design and simulation of a five degrees of freedom active control magnetic levitated motor. *IEEE Trans Magn* 2013; 49: 2257–2262.
7. Xiang B and Wong W. Electromagnetic vibration absorber for torsional vibration in high speed rotational machine. *Mech Syst Signal Process* 2020; 140.
8. Bangcheng H, Shiqiang Z, Xi W, et al. Integral design and analysis of passive magnetic bearing and active radial magnetic bearing for agile satellite application. *IEEE Trans Magn* 2011; 48: 1959–1966.
9. Jinji S, Yuan R and Jiancheng F. Passive axial magnetic bearing with Halbach magnetized array in magnetically suspended control moment gyro application. *J Magn Mater* 2011; 323: 2103–2107.
10. Yanliang X, Yueqin D, Xiuhe W, et al. Analysis of hybrid magnetic bearing with a permanent magnet in the rotor by FEM. *IEEE Trans Magn* 2006; 42: 1363–1366.

11. Jiancheng F, Jinji S, Yanliang X, et al. A new structure for permanent-magnet-biased axial hybrid magnetic bearings. *IEEE Trans Magn* 2009; 45: 5319–5325.
12. Na UJ. Design and analysis of a new permanent magnet biased integrated radial-axial magnetic bearing. *Int J Precis Eng Manuf* 2012; 13: 133–136.
13. Nagabhushan V and Fitz-Coy NG. On-orbit jitter control in momentum actuators using a three-flywheel system. *Acta Astronaut* 2014; 95: 61–81.
14. Zad HS, Khan TI and Lazoglu I. Design and adaptive sliding-mode control of hybrid magnetic bearings. *IEEE Trans Ind Electron* 2017; 65: 2537–2547.
15. Lu B, Choi H, Buckner GD, et al. Linear parameter-varying techniques for control of a magnetic bearing system. *Control Eng Pract* 2008; 16: 1161–1172.
16. Sahinkaya MN and Hartavi AE. Variable bias current in magnetic bearings for energy optimization. *IEEE Trans Magn* 2007; 43: 1052–1060.
17. Zhu K, Xiao Y and Rajendra AU. Optimal control of the magnetic bearings for a flywheel energy storage system. *Mechatronics* 2009; 19: 1221–1235.
18. Chen M and Knospe CR. Feedback linearization of active magnetic bearings: current-mode implementation. *IEEE ASME Trans Mechatron* 2005; 10: 632–639.
19. Hung JY, Albritton NG and Xia F. Nonlinear control of a magnetic bearing system. *Mechatronics* 2003; 13: 621–637.
20. Grabner H, Amrhein W, Silber S, et al. Nonlinear feedback control of a bearingless brushless DC motor. *IEEE ASME Trans Mechatron* 2009; 15: 40–47.
21. Chen S-L. Nonlinear smooth feedback control of a three-pole active magnetic bearing system. *IEEE Trans Control Syst Technol* 2010; 19: 615–621.
22. Fang J and Ren Y. Decoupling control of magnetically suspended rotor system in control moment gyros based on an inverse system method. *IEEE ASME Trans Mechatron* 2011; 17: 1133–1144.
23. Chen L, Zhu C, Zhong Z, et al. Radial position control for magnetically suspended high-speed flywheel energy storage system with inverse system method and extended 2-DOF PID controller. *IET Electr Power Appl* 2020; 14: 71–81.
24. Fang J, Zheng S and Han B. AMB vibration control for structural resonance of double-gimbal control moment gyro with high-speed magnetically suspended rotor. *IEEE ASME Trans Mechatron* 2011; 18: 32–43.
25. Xiang B and on Wong W. Vibration characteristics analysis of magnetically suspended rotor in flywheel energy storage system. *J Sound Vib* 2019; 444: 235–247.
26. Pappas P. The original Ampere force and Biot-Savart and Lorentz forces. *Il Nuovo Cimento B (1971-1996)* 1983; 76: 189–197.
27. Ravaud R, Lemarquand G and Lemarquand V. Force and stiffness of passive magnetic bearings using permanent magnets. Part 2: radial magnetization. *IEEE Trans Magn* 2009; 45: 3334–3342.
28. Isidori A. *Nonlinear control systems*. 3rd ed. Berlin Hong Kong: Springer Verlag, 1995.
29. Isidori A. *Nonlinear control system: an introduction*. 2nd ed. Berlin Hong Kong: Springer-Verlag, 1989.

Author biographies

Tong Wen was born in Hunan Province, in 1983. He received B.S degree and Ph.D. degree from Beijing University of Aeronautics and Astronautics, Beijing, China, in 2005 and 2012 respectively. He is now a lecturer and master tutor with School of Instrumentation and

Optoelectronic Engineering, Beihang University. His current research interests include the linear motor control, the control of the active magnetic bearing and magnetic suspension inertial stabilization platform used in the aviation remote sensing system.

Biao Xiang was born in 1987. He received the B.S. degree in physical and mechanical and electrical engineering from Xiamen University, Xiamen, China, and the M.S. degree in instrumentation science and opto-electronics engineering from Beihang University, Beijing, China. He is currently working toward the Doctoral degree in vibration analysis and control in the Department of Mechanical Engineering, Hong Kong Polytechnic University, Hong Kong. His research interests include active vibration analysis, measurement and control of high-speed motors.

Shilei Zhang was born in Shaanxi Province, in 1994. He received his B.S. degree from Nanjing University of Aeronautics and Astronautics, Nanjing, China, in 2017. Currently, he is studying at the School of Instrumentation and Optoelectronic Engineering, Beijing University of Aeronautics and Astronautics, Beijing, China. His research mainly concentrates on motor control.